JACS
JOURNAL OF THE AMERICAN CHEMICAL SOCIETY

Subscriber access provided by American Chemical Society

Article

Mechanistic Insights in Charge-Transfer-Induced Luminescence of 1,2-Dioxetanones with a Substituent of Low Oxidation Potential

Hiroshi Isobe, Yu Takano, Mitsutaka Okumura, Seiki Kuramitsu, and Kizashi Yamaguchi

J. Am. Chem. Soc., **2005**, 127 (24), 8667-8679• DOI: 10.1021/ja043295f • Publication Date (Web): 27 May 2005

Downloaded from http://pubs.acs.org on March 25, 2009

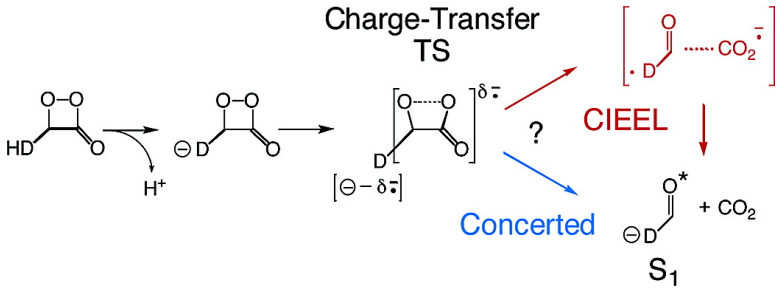

More About This Article

Additional resources and features associated with this article are available within the HTML version:

- Supporting Information
- Links to the 3 articles that cite this article, as of the time of this article download
- Access to high resolution figures
- Links to articles and content related to this article
- Copyright permission to reproduce figures and/or text from this article

View the Full Text HTML

ACS Publications
High quality. High impact.

Journal of the American Chemical Society is published by the American Chemical Society. 1155 Sixteenth Street N.W., Washington, DC 20036

J|A|C|S
ARTICLES
Published on Web 05/27/2005

Mechanistic Insights in Charge-Transfer-Induced Luminescence of 1,2-Dioxetanones with a Substituent of Low Oxidation Potential

Hiroshi Isobe,*,† Yu Takano,† Mitsutaka Okumura,† Seiki Kuramitsu,‡ and Kizashi Yamaguchi*,†

Contribution from the Department of Chemistry and Department of Biology, Graduate School of Science, Osaka University, Toyonaka, Osaka 560-0043, Japan

Received November 8, 2004; E-mail: isobe@chem.sci.osaka-u.ac.jp; yama@chem.sci.osaka-u.ac.jp

Abstract: We have investigated the decomposition pathway of dioxetanones **1c** with a phenoxide anion group by the B3LYP/6-31+G(d) method together with the second-order multireference Møller−Plesset perturbation (MRMP) theory and propose charge-transfer-induced luminescence (CTIL) with polarization-induced branching excitation processes. In the gas phase, the thermal decomposition of **1c** occurs by an asynchronous two-stage pathway without a discrete intermediate; that is, the initial O−O bond breaking to generate a charge-transfer (CT) diradical species is immediately followed by the subsequent C−C bond breaking with simultaneous back CT, which is responsible for the surface crossing at the avoided crossing. The activation energy is dramatically reduced from 19.4 to 3.8 kcal mol^{-1} by the deprotonation of phenol *meta*-**1d** to its anion *meta*-**1c**, showing an important role of the endothermic CT. The odd/even selection rule for the chemiluminescence efficiency can be explained by the orbital interaction for the back CT between the carbonyl π^* orbital and either a HOMO or a LUMO of the generated light emitters. To examine the accessibility of the chemically initiated electron exchange luminescence (CIEEL) route, we considered the solvent effects on the free-energy change of *meta*-**1c** by using continuum solvent models. The bending vibration mode of the CO_2 fragment is specifically considered. Borderline features emerges from the solution-phase CT reaction of *meta*-**1c**, which depends on the solvent polarity: one is a nonadiabatic or adiabatic back CT process (polarization-induced concerted CTIL), and the other is a radical dissociation, i.e., complete one-electron-transfer process (CIEEL).

Introduction

Chemiluminescence and bioluminescence have been widely recognized for their importance to a broad range of biological, chemical, and medical applications.[1] Although there is an astonishing diversity of bioluminescent organisms throughout terrestrial and aquatic environments, a unified picture at the chemical level has been elucidated:[2] all involve the formation and breakdown of a peroxide or hydroperoxide intermediate. Detailed knowledge of the decomposition processes of these species should provide the necessary mechanistic insights for the rational design of more effective chemiluminescence systems. We have explored the decomposition mechanisms of biologically important peroxides known as 1,2-dioxetanones (**1** and **3** in Chart 1) with ab initio computations.

There are two mechanistically distinct routes in the thermal generation of electronically excited products from dioxetanone and dioxetane derivatives.[3−6] The thermolysis of simple alkyl-substituted dioxetanones and dioxetanes produces two carbonyl compounds, one of which is electronically excited.[7] The ratio of triplet to singlet excited states is very high, so that the observed light emission is very weak. Both ab initio calcula-

Chart 1

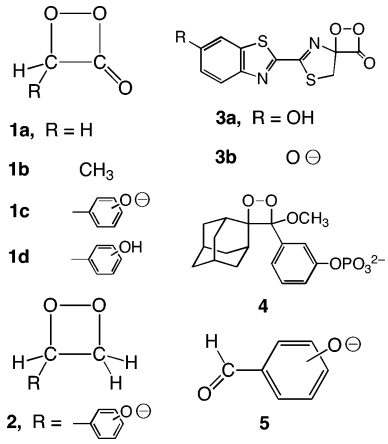

† Department of Chemistry.
‡ Department of Biology.

(1) (a) Beck, S.; Köster, H. *Anal. Chem.* **1990**, *62*, 2258. (b) Mayer, A.; Neuenhofer, S. *Angew. Chem., Int. Ed. Engl.* **1994**, *33*, 1044. (c) Adam, W.; Reinhardt, D.; Saha-Möller, C. R. *Analyst* **1996**, *121*, 1527.
(2) Hastings, J. W. *J. Mol. Evol.* **1983**, *19*, 309.
(3) McCapra, F. *Q. Rev. Chem. Soc.* **1966**, *20*, 485.
(4) Wilson, T. *Int. Rev. Sci., Phys. Chem. Ser. 2.* **1976**, *9*, 265.
(5) (a) Adam, W. *Pure Appl. Chem.* **1980**, *52*, 2591. (b) Adam, W.; Cilento, G. In *Chemical and Biological Generation of Excited States*; Academic: New York, 1982.
(6) Schuster, G. B. *Acc. Chem. Res.* **1979**, *12*, 366.

Scheme 1

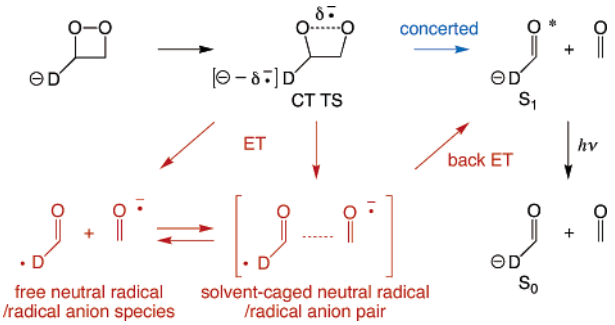

tions[8,9] and experimental evidence[7b,10] support that the stepwise diradical mechanism is operative for the reactions. In contrast, the chemically initiated electron exchange luminescence (CIEEL) mechanism has been proposed to account for the bright light emission involving the catalytic effect of an appropriate fluorescer with a low oxidation potential.[11] This phenomenon is generally observed in various chemiluminescence systems by either inter-[11−13] or intramolecular[14−21] electron-transfer processes. In the latter case, the primary electron transfer from an electron-donating group (D) to the O−O bond of peroxide provokes the decomposition of the peroxide into two radicals confined within a solvent cage, but from which it may diffuse freely (Scheme 1). The subsequent back electron transfer between the radicals releases enough energy to promote the fluorophore to its singlet excited state. The occurrence of the primary and subsequent electron-transfer processes is supported by kinetic[11−14] and viscosity dependence[15] studies.

Another origin for the high efficiency has been proposed as an alternative to the CIEEL mechanism, because there is some doubt about the efficiency of the back-electron-transfer process between the radicals in a solvent cage.[16] This constitutes the charge-transfer (CT) mechanism,[16−18] which assumes the rate-determining endothermic formation of a transition state with

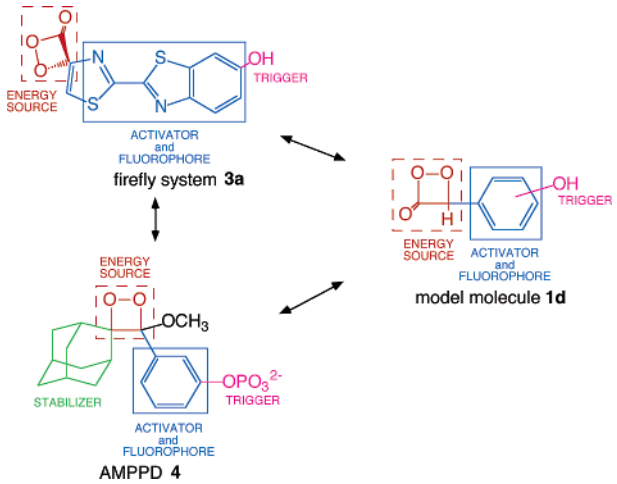

Figure 1. Three essential molecular components of the model molecule **1d**, dioxetanone intermediate **3a** of the firefly luciferin, and AMPPD **4**.[1c]

CT character. Directly, a CT excited state is generated immediately from the transition state during the decomposition process. The full charge development on the carbonyl fragment, the idea of complete electron transfer assumed in the CIEEL mechanism, is replaced with gradual charge development in the CT mechanism. We previously calculated the ionization potentials of monoanions of phenol, indole, and luciferins to estimate the CT excitation energy and distinguished between CT-induced luminescence (CTIL) through the CT complex and the CIEEL mechanism with the formation of a neutral radical/radical ion pair.[9] Since the above successive electron or charge-transfer processes are considered to occur very rapidly, such fast reactions cannot be directly observed in condensed phase by the available experimental techniques, and therefore, mechanistic information on the details of the reactions is limited. One of our goals is to determine the timing of the charge transfer and of the O−O and C−C bond cleavage to understand the chemiexcitation mechanism from the theoretical point of view.

Recently, novel highly efficient dioxetane systems with triggering functional groups have been rationally designed for commercial applications.[1,19−21] One of the most successful chemiluminescence systems in this area is 3-(2′-spiroadamantyl)-4-methoxy-4-(3′′-phosphoryloxy)-phenyl-1,2-dioxetane (AMPPD) (**4**) as a substrate for alkaline phosphotase.[19,20] There are some chemical equivalents between AMPPD and firefly systems, the latter being the most efficient light system in nature: (i) energy source, (ii) activator or fluorophore, and (iii) trigger as shown in Figure 1.[1c] The model molecules **1c** and **1d** used in this study were designed so as to have the bare essentials of the structural features (i)−(iii) inherent in the firefly luciferin. Our computations were also motivated by the desire to understand the origin of the structural and regioisomeric influence on the chemiluminescence properties of the species

(7) (a) Schmidt, S. P.; Schuster, G. B. *J. Am. Chem. Soc.* **1978**, *100*, 5559. (b) Adam, W.; Baader, W. J. *J. Am. Chem. Soc.* **1985**, *107*, 410.
(8) (a) Wilsey, S.; Bernardi, F.; Olivucci, M.; Robb, M. A.; Murphy, S.; Adam, W. J. *Phys. Chem. A* **1999**, *103*, 1669. (b) Tanaka, C.; Tanaka, J. *J. Phys. Chem. A* **2000**, *104*, 2078. (c) Rodríguez, E.; Reguero, M. *J. Phys. Chem. A* **2002**, *106*, 504.
(9) (a) Yamaguchi, K. In *Singlet Oxygen*; Frimer, A. A., Ed.; CRC Press: Boca Raton, FL, 1985; Vol. III, p 119. (b) Takano, Y.; Tsunesada, T.; Isobe, H.; Yoshioka, Y.; Yamaguchi, K.; Saito, I. *Bull. Chem. Soc. Jpn.* **1999**, *72*, 213.
(10) (a) O'Neal, H. E.; Richardson, W. H. *J. Am. Chem. Soc.* **1970**, *92*, 6553. (b) O'Neal, H. E.; Richardson, W. H. *J. Am. Chem. Soc.* **1971**, *93*, 1828. (c) O'Neal, H. E.; Richardson, W. H. *J. Am. Chem. Soc.* **1972**, *94*, 8665. (d) Richardson, W. H.; Montgomery, F. C.; Yelvington, M. B.; O'Neal, H. E. *J. Am. Chem. Soc.* **1974**, *96*, 7525. (e) Richardson, W. H.; Lovett, M. B.; Olson, L. *J. Org. Chem.* **1989**, *54*, 3523. (f) Wilson, T.; Golan, D. E.; Harris, M. S.; Baumstark, A. L. *J. Am. Chem. Soc.* **1976**, *98*, 1086. (g) Koo, K. Y.; Schuster, G. B. *J. Am. Chem. Soc.* **1977**, *99*, 5403.
(11) (a) Koo, J.-Y.; Schuster, G. B. *J. Am. Chem. Soc.* **1977**, *99*, 6107. (b) Koo, J.-Y.; Schuster, G. B. *J. Am. Chem. Soc.* **1978**, *100*, 4496. (c) Koo, J.-Y.; Schmidt, S. P.; Schuster, G. B. *Proc. Natl. Acad. Sci. U.S.A.* **1978**, *75*, 30.
(12) (a) Schmidt, S. P.; Schuster, G. B. *J. Am. Chem. Soc.* **1978**, *100*, 1966. (b) Schmidt, S. P.; Schuster, G. B. *J. Am. Chem. Soc.* **1980**, *102*, 306. (c) Schmidt, S. P.; Schuster, G. B. *J. Am. Chem. Soc.* **1980**, *102*, 7100. (d) Dixon, B. G.; Schuster, G. B. *J. Am. Chem. Soc.* **1979**, *101*, 3116.
(13) (a) Adam, W.; Simpson, G. A.; Yany, F. J. *Phys. Chem.* **1974**, *78*, 2559. (b) Adam, W.; Cueto, O.; Yany, F. J. *Am. Chem. Soc.* **1978**, *100*, 2587.
(14) (a) McCapra, F.; Beheshti, I.; Burford, A.; Hann, R. A.; Zaklika, K. A. *J. Chem. Soc., Chem. Commun.* **1977**, 944. (b) Zeklika, K. A.; Thayer, A. L.; Schaap, A. P. *J. Am. Chem. Soc.* **1978**, *100*, 4916. (c) Lee, C.; Singer, L. A. *J. Am. Chem. Soc.* **1980**, *102*, 3823.
(15) (a) Adam, W.; Bronstein, I.; Trofimov, A. V.; Vasil'ev R. F. *J. Am. Chem. Soc.* **1999**, *121*, 958. (b) Adam, W.; Trofimov, A. V. *J. Org. Chem.* **2000**, *65*, 6474. (c) Adam, W.; Matsumoto, M.; Trofimov, A. V. *J. Am. Chem. Soc.* **2000**, *122*, 8631.
(16) (a) Catalani, L. H.; Wilson, T. *J. Am. Chem. Soc.* **1989**, *111*, 2633. (b) Wilson, T. *Photochem. Photobiol.* **1995**, *62*, 601.
(17) White, E. H.; Roswell, D. F.; Dupont, A. C.; Wilson, A. A. *J. Am. Chem. Soc.* **1987**, *109*, 5189.
(18) (a) McCapra, F. *J. Photochem. Photobiol. A* **1990**, *51*, 21. (b) McCapra, F. *Tetrahedron. Lett.* **1993**, *34*, 6941.
(19) (a) Bronstein, I.; Edwards, B.; Voyta, J. C. *J. Biolumin. Chemilumin.* **1988**, *2*, 186. (b) Bronstein, I.; Edwards, B.; Voyta, J. C. *J. Biolumin. Chemilumin.* **1989**, *4*, 99. (c) Edwards, B.; Sparks, A.; Voyta, J. C.; Bronstein, I. *J. Biolumin. Chemilumin.* **1990**, *5*, 1. (d) Edwards, B.; Sparks, A.; Voyta, J. C.; Strong, R.; Murphy, O.; Bronstein, I. *J. Org. Chem.* **1990**, *55*, 6225.
(20) (a) Schaap, A. P.; Handley, R. S.; Giri, B. P. *Tetrahedron Lett.* **1987**, *28*, 935. (b) Schaap, A. P.; Chen, T. S.; Handley, R. S.; DeSylva, R.; Giri, B. P. *Tetrahedron Lett.* **1987**, *28*, 1155. (c) Schaap, A. P.; Sandison, M. D.; Handley, R. S. *Tetrahedron Lett.* **1987**, *28*, 1159.

with various substituents (R) in Chart 1. Specifically, we consider herein the dioxetanone functionality, because it has been suggested as a key high-energy intermediate responsible for light production in firefly and jellyfish biological systems.[22]

In this paper, we report hybrid density functional theory (DFT) and second-order multireference Møller−Plesset perturbation (MRMP) theory studies of the thermal decomposition mechanism of **1c**. First, the methodology used in our calculations is described. Next, the detailed results of the thermal CT reaction of *meta*-**1c** in the gas phase are presented. Third, comparisons between the *para* and *meta* regioisomers of **1c** are made, and their implications for the chemiluminescence properties are discussed from the viewpoint of the concerted CTIL mechanism. Fourth, whether the CIEEL mechanism operates for the thermal CT reaction of *meta*-**1c** is discussed within the polarizable-continuum model (PCM). Finally, some conclusions are briefly summarized.

Computational Details

To investigate the reaction mechanisms, we performed B3LYP/6-31+G(d) calculations,[26−29] unless otherwise specified. Stationary points on potential-energy surfaces were located by the energy gradient techniques, for which frequency analyses were carried out to characterize the nature of stationary points and to obtain the zero-point correction energies (ZPC) and the thermal corrections of the free energy at 298.15 K without scaling. Intrinsic reaction coordinate (IRC)[30] calculations were conducted to connect a transition structure to the reactants and products.

Restricted (R) DFT calculations perform well for the closed-shell reactants and products in Scheme 1. During the course of the reaction, however, RDFT molecular orbitals (MOs) should be reorganized into broken-symmetry (BS), unrestricted (U) DFT MOs, to describe appropriately strong charge transfer (CT) or open-shell character.[23] To obtain the symmetry-adapted (SA) picture for the broken-symmetry (BS) UDFT calculations, we used the natural orbitals (NOs) holding orbital symmetry, which are determined from the BS MOs. As shown previously,[24] the SA NOs of BS UDFT solutions can be determined by diagonalizing their spin-traced first-order density matrixes, as expressed in eq 1.

$$\rho(\mathbf{r}',\mathbf{r}) = \sum n_i \phi_i(\mathbf{r}')\, \phi_i^{\dagger}(\mathbf{r}) \qquad (1)$$

in which n_i denotes the occupation number of a NO ϕ_i, ranging from 0 to 2. The spin-polarized BS MOs ($\psi_i^{\pm}$) for the up-spin and down-spin states are derived by bonding (ϕ_i) and antibonding (ϕ_i^*) NOs, as shown in eq 2.

$$\psi_i^{\pm} = \cos\omega\, \phi_i \pm \sin\omega\, \phi_i^* \qquad (2)$$

in which ω is the orbital mixing coefficient; $\omega = 0°$ for closed-shell systems and $0° < \omega \le 45°$ for some strong donor−acceptor systems. In the latter case, the spatial separation of either spin orbital from the opposite spin orbital is responsible for CT diradical character. Since the strong CT interaction is accurately treated by the SA multiconfigurational wave functions, it is useful to define the common index between SA and BS approaches. For example, the diradical character (y_{HOMO}) is defined by the weight of the doubly excited configuration (W_{D}),[25] as given in eq 3, in which $T_{\mathrm{HOMO}} \equiv \langle \psi^{+}_{\mathrm{HOMO}} | \psi^{-}_{\mathrm{HOMO}} \rangle$ is the orbital overlap between the up-spin and down-spin orbitals defined in eq 2.

$$y_{\mathrm{HOMO}} = 2W_{\mathrm{D}} = \frac{{n_{\mathrm{HOMO}}}^2 - 4n_{\mathrm{HOMO}} + 4}{{n_{\mathrm{HOMO}}}^2 - 2n_{\mathrm{HOMO}} + 2}\,(\mathrm{SA}) = 1 - \frac{2T_{\mathrm{HOMO}}}{1 + {T_{\mathrm{HOMO}}}^2}\,(\mathrm{BS}) \qquad (3)$$

The y_{HOMO} value is 100% for complete one-electron-transfer (ET) diradical formation, for which T_{HOMO} is zero, whereas y_{HOMO} is 0% for a closed-shell configuration, for which T_{HOMO} becomes 1.0, and therefore, the up-spin and down-spin orbitals are equivalent to the closed-shell orbitals. The diradical character can be used as a chemical criterion for the formation of a diradical by one-electron transfer in the ground state.

To depict the energy levels of the excited states, we calculated vertical excitation energies at the B3LYP optimized geometries by the second-order multireference Møller−Plesset perturbation (MRMP) theory[31] with the 6-31+G(d) basis set. The reference functions were obtained by the state-averaged complete-active-space, self-consistent field (CASSCF) calculations.[32] The active space used for **1c** is schematically illustrated in Chart 2 (left). In this active space, 12 electrons are placed in the nine valence bonding and antibonding π orbitals of oxybenzaldehyde, the nonbonding orbital of the carbonyl group, and the LUMO of the CO_2 fragment, which is labeled as $\{12,11\}_{\mathrm{CC}}$. This active space can handle the C−C bond-breaking step of **1c**, which is of particular interest in relation to the excitation mechanism. To check the validity of the size of the active space employed, we have extensively tested several different active spaces and found that the correlation of the lone pairs on the oxygen atoms of the peroxide bond is dynamical rather than nondynamical for the ground

Chart 2

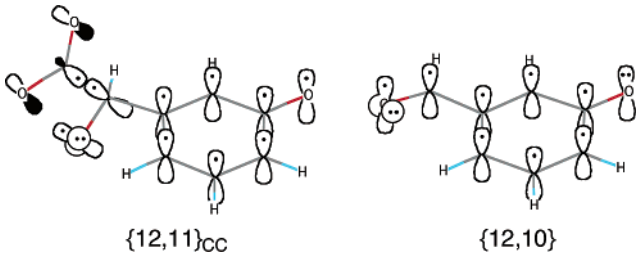

(21) (a) Matsumoto, M.; Watanabe, N.; Kobayashi, H.; Azami, M.; Ikawa, H. *Tetrahedron Lett.* **1997**, *38*, 411. (b) Matsumoto, M.; Watanabe, N.; Shiono, T.; Suganuma, H.; Matsubara, J. *Tetrahedron Lett.* **1997**, *38*, 5825. (c) Matsumoto, M.; Ishihara, T.; Watanabe, N.; Hiroshima, T. *Tetrahedron Lett.* **1999**, *40*, 4571. (d) Watanabe, N.; Suganuma, H.; Kobayashi, H.; Mutoh, H.; Katao, Y.; Matsumoto, M. *Tetrahedron Lett.* **1999**, *55*, 4287. (e) Watanabe, N.; Kobayashi, H.; Azami, M.; Matsumoto, M. *Tetrahedron Lett.* **1999**, *55*, 6831.

(22) (a) Goto, T.; Kishi, Y. *Angew. Chem., Int. Ed. Engl.* **1968**, *7*, 407. (b) White, E. H.; Miano, J. D.; Umbreit, M. *J. Am. Chem. Soc.* **1975**, *97*, 198. (c) McCapra, F. *Acc. Chem. Res.* **1976**, *9*, 201.

(23) (a) Takabe, T.; Yamaguchi, K. *Chem. Phys. Lett.* **1976**, *40*, 347. (b) Takabe, T.; Takenaka, K.; Yamaguchi, K.; Fueno, T. *Chem. Phys. Lett.* **1976**, *44*, 65. For the interrelationship between MO and CT theories, see Supporting Information.

(24) (a) Yamaguchi, K. *Chem. Phys. Lett.* **1975**, *33*, 330. (b) Yamaguchi, K. In *Self-Consistent Field Theory and Applications*; Carbo, R.; Klobukowski, M., Eds.; Elsevier: Amsterdam, 1990. (c) Yamaguchi, K.; Okumura, M.; Takada, K.; Yamanaka, S. *Int. J. Quantum Chem., Quantum Chem. Symp.* **1993**, *27*, 501.

(25) (a) Isobe, H.; Takano, Y.; Kitagawa, Y.; Kawakami, T.; Yamanaka, S.; Yamaguchi, K.; Houk, K. N. *Mol. Phys.* **2002**, *100*, 717. (b) Isobe, H.; Takano, Y.; Kitagawa, Y.; Kawakami, T.; Yamanaka, S.; Yamaguchi, K.; Houk, K. N. *J. Phys. Chem. A* **2003**, *107*, 682. (c) Isobe, H.; Yamanaka, S.; Yamaguchi, K. *Int. J. Quantum Chem.* **2003**, *95*, 532.

(26) Becke, A. D. *Phys. Rev. A* **1988**, *38*, 3098. (b) Lee, C.; Yang, W.; Parr, R. G. *Phys. Rev. B* **1988**, *37*, 785. (c) Becke, A. D. *J. Chem. Phys.* **1993**, *98*, 5648.

(27) Hariharan, P. C.; Pople, J. A. *Theor. Chim. Acta* **1973**, *28*, 213.

(28) Clark, T.; Chandrasekhar, J.; Spitznagel, G. W.; Schleyer, P. v. R. *J. Comput. Chem.* **1983**, *4*, 294.

(29) Frisch, M. J.; Pople, J. A.; Binkley, J. S. *J. Chem. Phys.* **1984**, *80*, 3265.

(30) (a) Gonzalez, C.; Schlegel, H. B. *J. Chem. Phys* **1989**, *90*, 2154. (b) Gonzalez, C.; Schlegel, H. B. *J. Phys. Chem.* **1990**, *94*, 5523.

(31) (a) Hirao, K. *Chem. Phys. Lett.* **1992**, *190*, 374. (b) Hirao, K. *Chem. Phys. Lett.* **1992**, *196*, 397. (c) Hirao, K. *Int. J. Quantum Chem.* **1992**, *S26*, 517. (d) Hirao, K. *Chem. Phys. Lett.* **1993**, *201*, 59.

(32) (a) Siegbahn, P. E.; Heiberg, A.; Roos, B. O.; Levy, B. *Phys. Scr.* **1980**, *21*, 323. (b) Roos, B. O.; Taylor, P. R.; Siegbahn, P. E. *Chem. Phys.* **1980**, *48*, 157. (c) Roos, B. O. *Int. J. Quantum Chem.* **1980**, *S14*, 175.

state, but the nonbonding orbital of the carbonyl group makes a substantial contribution to the excitation energy of a diradical species due to an excitation from the nonbonding orbital. For the detailed results, see the Supporting Information.

We considered the solvent effects on the reaction mechanism by using the continuum solvent model. The geometries of reactants, transition structures, and products in solutions were optimized by the polarizable-continuum model (PCM)[33] or Onsager model[34] with dielectric constants (ϵ) of 2.25 (benzene) and 46.70 (DMSO). The free energies of solvation (ΔG_{solv}), which include cavitation, dispersion, and repulsion contributions at 298.15 K, were calculated by PCM HF/6-31+G(d), unless otherwise specified. The free energy of a species, here denoted generally by A, relative to the equilibrium geometry (min.) (ΔG) was evaluated according to eq 4,[35] in which ΔG_{gas} is the free energy of A relative to the minimum in the gas phase, calculated by B3LYP/6-31+G(d).

$$\Delta G = \Delta G_{gas} + \Delta G_{solv}(A) - \Delta G_{solv}(min.) \quad (4)$$

All DFT calculations were carried out with Gaussian 94 and 98.[36] The GAMESS program package[37] was used for MRMP calculations.

Results and Discussion

CT-Induced Decomposition Mechanism of 1,2-Dioxetanone. We have explored the IRC path for the decomposition reaction of *meta*-**1c** to clarify the characteristics of the charge-transfer (CT)-induced decomposition mechanism. The IRC path for *meta*-**1c** is summarized in Figure 2. The top panel shows the potential-energy profile of the S_0 IRC path, together with the T_1 and S_1 potential-energy changes as a function of the reaction coordinate (s). The vertical energy gaps between the ground state and first singlet excited states were estimated by using the MRMP $\{12,11\}_{CC}$ calculations. In the second, third, and bottom panels in Figure 2A are drawn the variations of the O−O and C−C bond lengths (r), total Mulliken charge density of the dioxetanone functionality (ρ_{DON}) and the CO_2 fragment (ρ_{CO2}), and the diradical character (y_{HOMO}) that results from the S_0 IRC path. The reaction proceeds with CT through a slightly endothermic transition structure (TS). As displayed in Figure 3, this CT TS has an almost planar OCCO ring, which is maintained throughout the IRC path, with a slightly elongated (by 0.17 Å) O−O bond from the equilibrium geometry (min.). The most prominent feature of these computations is the torsional motion about the C_6−C_1 bond, since the dihedral angle C_7C_6−C_1O_3 changes from 122.7° (min.) to 140.8° (CT TS), to acquire the appropriate conformation of the aromatic ring for

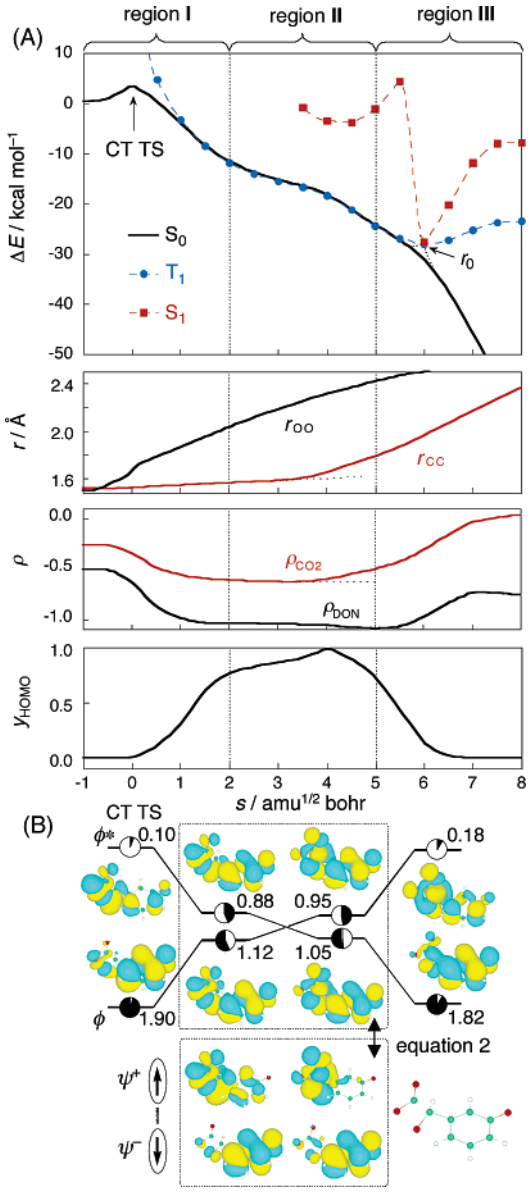

Figure 2. (A) Energy profiles of the IRC path that starts from the CT TS of *meta*-**1c**, calculated by B3LYP/6-31+G(d), and the T_1 and S_1 energy changes along the IRC path (top); the S_0/S_1 vertical excitation energies were calculated by the MRMP$\{12,11\}_{CC}$/6-31+G(d) method; variations of the C−C (r_{CC}) and O−O (r_{OO}) bond distances along the IRC path (second); variations of the total Mulliken charge densities of the dioxetanone (ρ_{DON}) and CO_2 (ρ_{CO2}) moieties along the IRC path (third); variation of the diradical character (y_{HOMO}) along the IRC path (bottom). (B) Changes in the shapes of natural orbitals for the HOMO and LUMO of *meta*-**1c** and their occupation numbers along the IRC path; the first column is presented for the CT TS, the second for the structure at 2.0 amu$^{1/2}$ bohr, the third for the structure at 4.5 amu$^{1/2}$ bohr, and the fourth for the structure at 6.5 amu$^{1/2}$ bohr; the first row is depicted for the LUMO, the second for the HOMO, the third for the up-spin orbital (ψ^+), and the fourth for the down-spin orbital (ψ^-); C, O, and H atoms are shown in green, red, and gray; the occupation numbers of the HOMO and LUMO are illustrated by shaded circles.

(33) (a) Miertus, S.; Scrocco, E.; Tomasi, J. *Chem. Phys.* **1981**, *55*, 117. (b) Miertus, S.; Tomasi, J. *Chem. Phys.* **1982**, *65*, 239. (c) Cossi, M.; Barone, V.; Cammi, R.; Tomasi, J. *Chem. Phys. Lett.* **1996**, *255*, 327. (d) Barone, V.; Cossi, M.; Mennucci, B.; Tomasi, J. *J. Chem. Phys.* **1997**, *107*, 3210.
(34) (a) Wong, M. W.; Frisch, M. J.; Wiberg, K. B. *J. Am. Chem. Soc.* **1991**, *113*, 4776. (b) Wong, M. W.; Wiberg, K. B.; Frisch, M. J. *J. Am. Chem. Soc.* **1992**, *114*, 523. (c) Wong, M. W.; Wiberg, K. B.; Frisch, M. J. *J. Chem. Phys.* **1991**, *95*, 8991. (d) Wong, M. W.; Wiberg, K. B.; Frisch, M. J. *J. Am. Chem. Soc.* **1992**, *114*, 1645.
(35) Levine, I. N. In *Quantum Chemistry Fifth Edition*; Prentice Hall: 2000; p 593.
(36) (a) Frisch, M. J.; Trucks, G. W.; Schlegel, H. B.; Gill, P. M. W.; Johnson, B. G.; Robb, M. A.; Cheeseman, J. R.; Keith, T. A.; Petersson, G. A.; Montgomery, J. A.; Raghavachari, K.; Al-Laham, M. A.; Zakrzewski, V. G.; Ortiz, J. V.; Foresman, J. B.; Cioslowski, J.; Stefanov, B. B.; Nanayakkara, A.; Challacombe, M.; Peng, C. Y.; Ayala, P. Y.; Chen, W.; Wong, M. W.; Andres, J. L.; Replogle, E. S.; Gomperts, R.; Martin, R. L.; Fox, D. J.; Binkley, J. S.; Defrees, D. J.; Baker, J.; Stewart, J. P.; Head-Gordon, M.; Gonzalez, C.; Pople, J. A. *Gaussian 94*, Revision E.3; Gaussian, Inc.: Pittsburgh, PA, 1995. (b) Frisch, M. J.; Trucks, G. W.; Schlegel, H. B.; Scuseria, G. E.; Robb, M. A.; Cheeseman, J. R.; Zakrzewski, V. G.; Montgomery, J. A., Jr.; Stratmann, R. E.; Burant, J. C.; Dapprich, S.; Millam, J. M.; Daniels, A. D.; Kudin, K. N.; Strain, M. C.; Farkas, O.; Tomasi, J.; Barone, V.; Cossi, M.; Cammi, R.; Mennucci, B.; Pomelli, C.; Adamo, C.; Clifford, S.; Ochterski, J.; Petersson, G. A.; Ayala, P. Y.; Cui, Q.; Morokuma, K.; Malick, D. K.; Rabuck, A. D.; Raghavachari, K.; Foresman, J. B.; Cioslowski, J.; Ortiz, J. V.; Stefanov, B. B.; Liu, G.; Liashenko, A.; Piskorz, P.; Komaromi, I.; Gomperts, R.; Martin, R. L.; Fox, D. J.; Keith, T.; Al-Laham, M. A.; Peng, C. Y.; Nanayakkara, A.; Gonzalez, C.; Challacombe, M.; Gill, P. M. W.; Johnson, B.; Chen, W.; Wong, M. W.; Andres, J. L.; Gonzalez, C.; Head-Gordon, M.; Replogle, E. S.; Pople, J. A. *Gaussian 98*, Revision A.6; Gaussian, Inc.: Pittsburgh, PA, 1998.
(37) Schmidt, M. W.; Baldridge, K. K.; Boatz, J. A.; Elbert, S. T.; Gordon, M. S.; Jensen, J. J.; Koseki, S.; Matsunaga, N.; Nguyen, K. A.; Su, S.; Windus, T. L.; Dupuis, M.; Montgomery, J. A. *J. Comput. Chem.* **1993**, *14*, 1347.

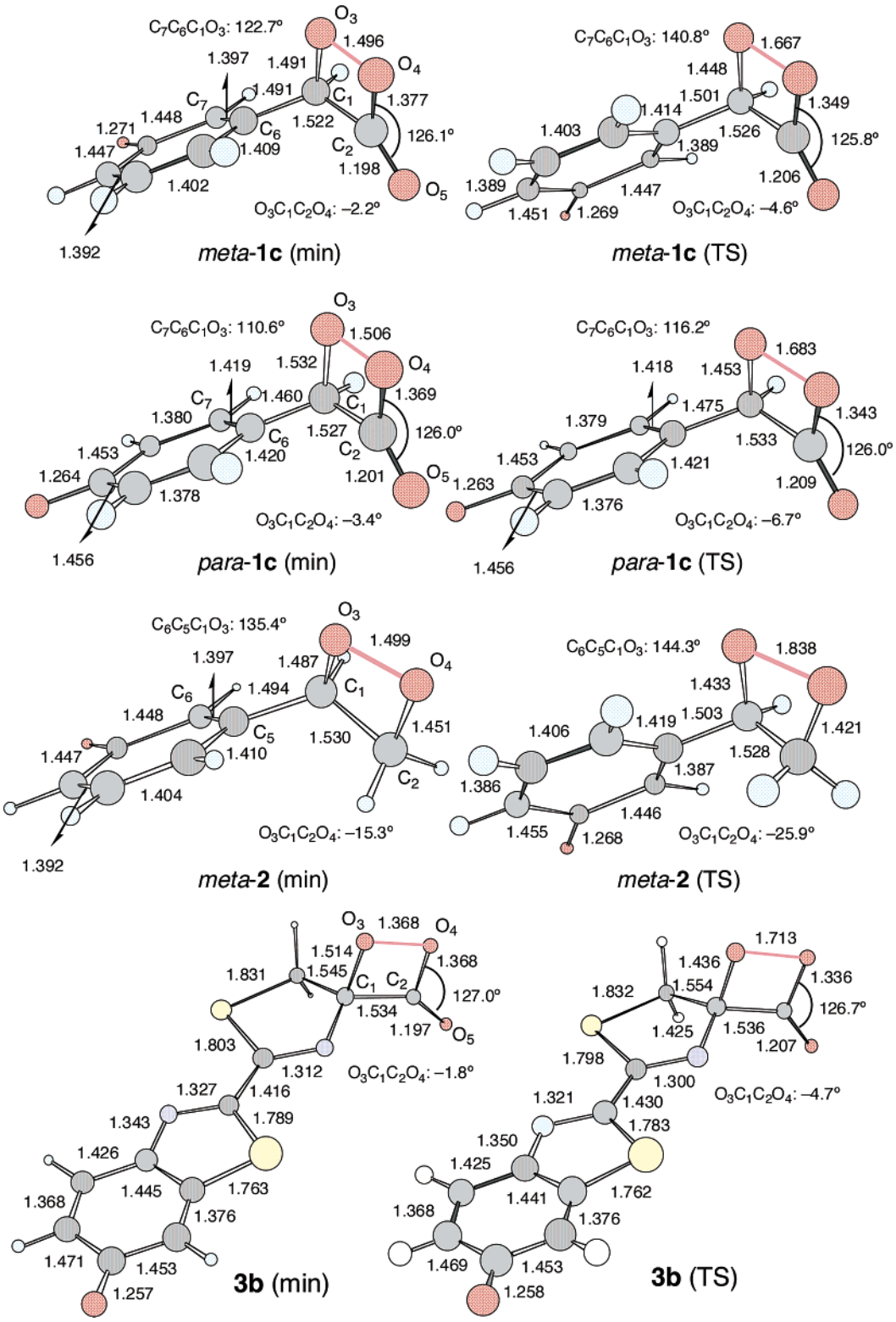

Figure 3. Optimized geometrical parameters calculated by the B3LYP/6-31+G(d) method; bond lengths are given in angstroms.

effective CT interaction. The CT is coupled with the dissociation of the peroxide bond and the conformational alignment of the electron-donor part. This result is consistent with the experimental observation that the rotational hindrance of the electron-donating group makes the half-life of emission far longer.[21b]

To investigate the energetics of the thermal CT reaction of *meta*-**1c** in the gas phase, the possible decomposition products (neutral and anionic forms of *meta*-oxybenzaldehyde **5** and CO_2) were optimized for the isolated molecules, at the B3LYP/6-31+G(d) level. We also performed geometry optimization for the first singlet excited state of the *meta*-**5** anion by the CI with the singles (CIS)/6-31+G(d) method to estimate adiabatic excitation energy of *meta*-**5** anion. The MRMP procedure was applied to the ground and excited states separately, based on the CASSCF wave function, in which 12 active electrons are distributed in the nine valence π orbitals and the nonbonding

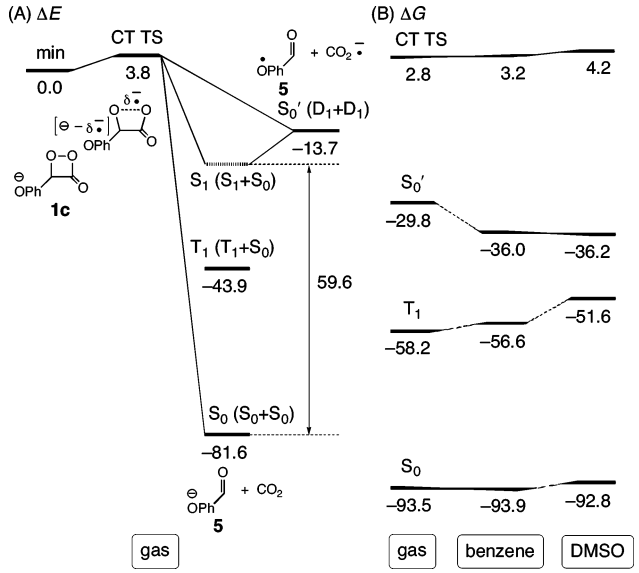

Figure 4. (A) Energy diagram for the thermal CT decomposition of *meta*-**1c** in the gas phase, as calculated by B3LYP/6-31+G(d); the S_0/S_1 adiabatic excitation energy of *meta*-**5** was calculated at the MRMP{12,10}/6-31+G-(d) level by using the S_1 optimized geometry of *meta*-**5** at the CIS/6-31+G-(d) level; the relative energies (ΔE) are given in kcal mol^{-1}. (B) Free-energy diagram of the decomposition products of *meta*-**1c** in the benzene and DMSO media, as obtained by eq 4; solvation free energies of the CT TSs and decomposition products were evaluated by PCM B3LYP/6-31+G-(d)[50] and PCM HF/6-31+G(d); the relative free energies (ΔG) are given in kcal mol^{-1}; the values for the S_0 and T_1 states are calculated for *meta*-**5** (S_0) + CO_2 (S_0) and *meta*-**5** (T_1) + CO_2 (S_0) as free anion/neutral species and the values for the S_0' states are for *meta*-**5** (D_1) + CO_2 (D_1) as free neutral radical/radical anion species.

orbital of the carbonyl group as depicted in Chart 2 (right). The obtained energy diagram is summarized in Figure 4A. The energy released from the CT TS in the reaction (85.4 kcal mol^{-1}) is sufficient to generate not only the singlet excited state of the *meta*-**5** anion and ground state of neutral CO_2 (S_1, 59.6 kcal mol^{-1}) but also two doublet states of the neutral *meta*-**5** and CO_2 anion (S_0', 67.9 kcal mol^{-1}), which can form an excited emitter, as shown in Figure 4A.

In view of the variations in the ρ_{DON} and y_{HOMO} values along the IRC path, it seems reasonable to consider the reaction mechanism for the three distinct regions indicated in Figure 2A: (I) CT region ($s < 2$ amu$^{1/2}$ bohr), (II) one-electron-transfer (ET) region ($2 < s < 5$ amu$^{1/2}$ bohr), and (III) back CT region ($s > 5$ amu$^{1/2}$ bohr). This will be discussed separately.

(A) Region I: CT-Induced O−O Bond Dissociation. The B3LYP calculations show that the activation energies of the decomposition of *meta*-**1c** are 3.8 (ΔE), 2.7 (ΔE + ZPC), and 0.9 (ΔE + ZPC + approximate spin projection) kcal mol^{-1}, in contrast to 16.9−19.4 kcal mol^{-1} for the neutral dioxetanone *meta*-**1d** (Table 1). The large difference is due to the ionization potential (I_p) of the electron-donating group (R in Chart 1); the I_p values of phenol and its monoanion are 8.50 and 2.24 eV at the B3LYP/6-311+G(d) level. The deprotonation of the phenolic OH group plays a crucial role in the CT mechanism for *meta*-**1c**; however, the CT cannot be spontaneous. Even though a good electron-donating substituent (the phenoxide anion) is involved, the electron affinity (E_a) of the dioxetanone peroxide bond is quite negative at the equilibrium geometry[38] (in this case, $\gamma > 0$ in eq S7). The O−O bond elongation causes a drastic increase in the electron affinity of the dioxetanone functionality to form the endothermic CT TS.

For a better understanding of the CT mechanism, we have analyzed the natural orbitals (NOs) of the broken-symmetry (BS) B3LYP solutions. Changes in the shapes of valence NOs (HOMO and LUMO) and their occupation numbers along the IRC path are selectively indicated in Figure 2B; note that the occupation numbers for the other NOs are close to 0.0 or 2.0, as shown in Table S1 (Supporting Information). The small CT character ($\Delta\rho_{DON} = -0.12$) at the CT TS is due to the weak interaction between the HOMO of the phenoxide anion and the antibonding σ^* orbital of the O−O bond. Also, the decrease in the HOMO/LUMO gap, caused by the O−O elongation, induces a small amount of CT excitation (small occupation of the LUMO), which results in a low ET diradical character ($y_{HOMO} = 0.5\%$) at the CT TS and little weakening of the O−O bond. Subsequently, further O−O breaking leads to a stronger CT interaction and prominent diradical character, with considerable stabilization of the system. The CT and diradical generation cooperatively provoke an irreversible O−O bond breaking, in accordance with previous MO calculations.[9,39] Consequently, full ET ($\rho_{DON} \cong -1.0$) is achieved just before the system enters the region II, in which the strong diradical character ($y_{HOMO} > 80\%$) is maintained until s reaches 5 amu$^{1/2}$ bohr.

To elucidate the difference of electron-accepting ability between the dioxetanone and dioxetane structures, B3LYP calculations were performed to locate the CT TS for the decomposition reaction of the dioxetane model *meta*-**2**. As displayed in Figure 3, the OCCO ring of *meta*-**2** is twisted by 15.3° and 25.9° at the equilibrium geometry and the CT TS. The intramolecular CT plays an important role in the acceleration of the reaction; however, the CT TS was located to be relatively late (ΔE + ZPC = 8.0 kcal mol^{-1}, $\Delta\rho_{DON} = -0.25$, and $y_{HOMO} = 3.8\%$) compared with that of dioxetanone *meta*-**1c**. This is due to the smaller electron affinity of the dioxetane ring by 0.71 ($r_{OO} = 1.5$ Å) and 1.2 eV ($r_{OO} > 2.0$ Å).[38] Thus, the *meta*-**2** molecule must undergo considerable O−O elongation ($\Delta r_{OO} = 1.84$ Å) from its equilibrium geometry to form the CT TS; indeed, one-electron transfer is energetically unfavorable for *meta*-**2** even at the geometry with complete O−O bond cleavage. In contrast, on account of the large exothermicity for the primary ET process of the *meta*-**1c** dioxetanone, the CT TS is achieved exceedingly early (ΔE + ZPC = 2.7 kcal mol^{-1}, $\Delta r_{OO} = 0.17$ Å, $\Delta\rho_{DON} = -0.12$, and $y_{HOMO} = 0.51\%$) on the reaction pathway.[40] From this viewpoint, we emphasize the utility of the dioxetanone functionality in regard to generating a high luminescence reactivity, because its short lifetime of decomposition may suppress any proton transfer from the environment, which would severely impede the CT-induced decomposition of anion species.

It is meaningful to mention here the decomposition mechanism of the dioxetanone intermediate **3**, which is assumed to be formed by the luciferase-catalyzed multistep oxidation of the luciferin in the firefly system,[41] in relation to the model

(38) The variations in the vertical electron affinity of the dioxetanone and dioxetane functionalities as a function of the O−O bond distance are summarized in Figure S6 (Supporting Information).
(39) Schmidt, S. P.; Vincent, M. A.; Dykstra, C. E.; Schuster, G. B. *J. Am. Chem. Soc.* **1981**, *103*, 1292.
(40) Hammond, G. S. *J. Am. Chem. Soc.* **1955**, *77*, 334.
(41) (a) Deluca, M.; McElroy, W. D. *Biochemistry* **1974**, *13*, 921. (b) McElroy, W. D.; Seliger, H. H.; White, E. H. *Photochem. Photobiol.* **1969**, *10*, 153. (c) White, E. H.; Steinmetz, M. G.; Miano, J. D.; Wildes, P. D.; Moreland, R. *J. Am. Chem. Soc.* **1980**, *102*, 3199. (d) White, E. H.; Roswell, D. F. *Photochem. Photobiol.* **1991**, *53*, 131.

Table 1. Relative Energies, C−C and O−O Bond Distance, Diradical Characters, Mulliken Charge, and Spin Densities of the Critical Points for the Decomposition Reactions of Dioxetanones 1, Dioxetane 2, and Dioxetanone Intermediates 3 of the Firefly Luciferin, Calculated by B3LYP/6-31+G(d)

						Mulliken charge density (spin density)[d]					
state	ΔE[a]	ΔE + ZPC[a]	r_{CC}[b]	r_{OO}[b]	y_{HOMO}[c]	C_1	C_2	O_3	O_4	O_5	ρ_{DON}
meta-**1c** (min.)	0.0	0.0	1.522	1.496	0.0	−0.23	0.25	−0.17	−0.15	−0.43	−0.51
						(0.00)	(0.00)	(0.00)	(0.00)	(0.00)	(0.00)
meta-**1c** (TS)	3.8	2.7(0.9)	1.526	1.667	0.5	−0.25	0.31	−0.23	−0.21	−0.44	−0.63
						(−0.01)	(0.00)	(0.12)	(0.10)	(0.00)	(0.23)
meta-**1c**	−12.2		1.553	2.000	25.0	−0.18	0.29	−0.36	−0.38	−0.51	−0.98
						(−0.04)	(0.01)	(0.61)	(0.32)	(0.07)	(0.98)
meta-**1c** (P[e])	−81.6	−83.3									
para-**1c** (min.)	0.0	0.0	1.527	1.506	0.0	−0.41	0.27	−0.16	−0.16	−0.44	−0.70
						(0.00)	(0.00)	(0.00)	(0.00)	(0.00)	(0.00)
para-**1c** (TS)	2.2	1.4(0.5)	1.533	1.683	0.1	−0.34	0.27	−0.19	−0.23	−0.46	−0.77
						(0.02)	(0.00)	(0.08)	(0.09)	(0.00)	(0.21)
para-**1c**	−11.3		1.577	2.000	20.8	−0.28	0.37	−0.34	−0.37	−0.50	−0.95
						(0.00)	(−0.03)	(0.64)	(0.26)	(0.05)	(0.90)
para-**1c** (P[e])	−85.8	−87.1									
meta-**1d** (min.)	0.0	0.0	1.527	1.496	0.0	−0.16	0.30	−0.17	−0.11	−0.39	−0.31
						(0.00)	(0.00)	(0.00)	(0.00)	(0.00)	(0.00)
meta-**1d** (TS)	19.4	17.0(16.9)	1.564	2.035	20.8	−0.21	0.33	−0.17	−0.14	−0.35	−0.32
						(0.02)	(−0.09)	(−0.57)	(0.62)	(−0.04)	(−0.09)
meta-**1d** (P[e])	−84.0	−85.9									
meta-**2** (min.)	0.0	0.0	1.530	1.499	0.0	−0.17	−0.38	−0.19	−0.22		−0.41
						(0.00)	(0.00)	(0.00)	(0.00)		(0.00)
meta-**2** (TS)	9.5	8.0(6.0)	1.528	1.838	3.8	−0.08	−0.39	−0.32	−0.32		−0.66
						(0.01)	(0.02)	(0.18)	(0.28)		(0.49)
meta-**2**	7.69		1.530	2.000	25.0	0.00	−0.40	−0.40	−0.37		−0.78
						(0.01)	(0.02)	(0.29)	(0.48)		(0.79)
meta-**2** (P[e])	−63.9	−68.0									
3a (min.)	0.0	0.0	1.420	1.496	0.0	−0.02	0.40	−0.16	−0.15	−0.38	−0.31
						(0.00)	(0.00)	(0.00)	(0.00)	(0.00)	(0.00)
3a (TS)	19.7	17.3(16.3)	1.422	2.053	21.2	0.09	0.45	−0.20	−0.15	−0.36	−0.17
						(0.02)	(−0.09)	(−0.61)	(0.63)	(−0.03)	(−0.08)
3a (P[e])	−92.3	−93.7									
3b (min.)	0.0	0.0	1.534	1.496	0.0	−0.18	0.33	−0.16	−0.17	−0.42	−0.61
						(0.00)	(0.00)	(0.00)	(0.00)	(0.00)	(0.00)
3b (TS)	5.1	4.0(1.8)	1.536	1.713	1.0	−0.14	0.37	−0.21	−0.24	−0.44	−0.66
						(0.03)	(0.01)	(0.14)	(0.13)	(0.01)	(0.31)
3b	−4.9		1.551	2.000	67.1	0.09	0.47	−0.36	−0.38	−0.52	−0.71
						(−0.02)	(0.00)	(0.56)	(0.33)	(0.07)	(0.94)
3b (P[e])	−92.9	−94.1									

[a] Energies (ΔE) and energies including zero-point corrections (ΔE + ZPC) are in kcal mol^{-1} relative to the equilibrium geometry (min.); the values in parentheses are after approximate spin projection (see eqs S14 in Supporting Information). [b] C_1-C_2 (r_{CC}) and O_3-O_4 (r_{OO}) bond lengths are in angstroms. [c] Diradical characters (y_{HOMO}) are in %. [d] Site numbers of skeletal parts are shown in Figure 3; ρ_{DON} is the total Mulliken charge density of the dioxetanone (or dioxetane) functionality. [e] P denotes decomposition products in the ground state.

molecule **1c**. Very recently, Orlova et al.[42] investigated the reaction mechanisms for the formation of the keto form of oxyluciferin from the firefly luciferin with the B3LYP/6-31G-(d) method. It was found that the decomposition reaction of the peroxylactone with a thiazole fragment void of an electron-donating group proceeds in one step through a singlet diradical TS, with an activation barrier of 18.1 kcal mol^{-1} and a high exothermicity of 90.8 kcal mol^{-1}. Their result is similar to our homolytic diradical TS of *meta*-**1d** in Table 1. We also located the TSs for the O−O breaking of the complete luciferin structures given by the molecules **3a** and **3b** at the B3LYP/6-31+G(d) level, as shown in Figure 3 and Table 1. The activation energy of protonated peroxylactone **3a** (17.3 kcal mol^{-1}) is still at the same level as the peroxylactone with a thiazole fragment and *meta*-**1d**. In contrast, the activation energy of deprotonated peroxylactone **3b** is substantially reduced to 4.0 kcal mol^{-1} because of the CT from the oxy-substituted benzthiazoline to the dioxetanone functionality with the elongated peroxide bond, which emphasizes the importance of the presence of an easily oxidized substituent in such chemiluminescence reactions.

(B) Region II: Conversion of the ET Diradical Configuration. In region II, the NOs for HOMO and LUMO of *meta*-**1c** are delocalized over the entire molecule due to the strong interaction between the HOMO of phenoxide anion and the O−O σ^* orbital, as shown in Figure 2B. The occupation numbers of these NOs are fairly close to 1.0, which indicates that the system possesses substantial diradical character; the HOMO/LUMO switching occurs smoothly at around $s = 4$ amu$^{1/2}$ bohr. For such an open-shell configuration, the localized MO description is useful for intuitive interpretation. We depict the spin-polarized BS MOs for the up and down spin states (ψ^+ and ψ^-) in Figure 2B, by mixing the paired NOs (ϕ^* and ϕ) according to eq 2. The orbital overlaps $\langle\psi^+|\psi^-\rangle$ ($\equiv T$) between the spin-polarized MOs are 0.12 and 0.05 at $s = 2$ and 4.5 amu$^{1/2}$ bohr. The up-spin and down-spin orbitals are essentially localized on the dioxetanone and phenoxide parts, which shows the intramolecular-type ET diradical character.

(42) Orlova, G.; Goddard, J. D.; Brovko, L. Y. *J. Am. Chem. Soc.* **2003**, *125*, 6962.

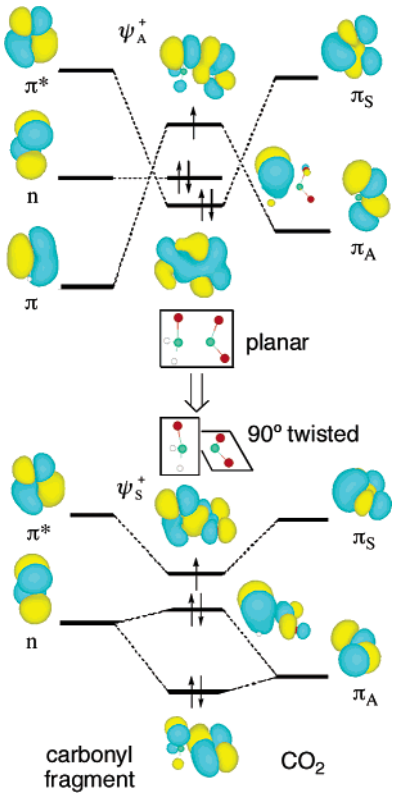

Figure 5. Schematic illustration of the MO correlation diagram of **1a** with planar and 90° twisted structures; C, O, and H atoms are shown in green, red, and gray.

Further inspection reveals the change in the orbital-phase relation of the up-spin orbital (ψ^+) in region II. For proper understanding of the ψ^+ orbital change in the strong diradical region, we consider the orbital correlation diagram for the anion doublet state of the dioxetanone skeleton as illustrated in Figure 5. From Figure 5, we see that at the beginning of the diradical region the unpaired electron is mainly distributed over the π orbital of carbonyl fragment and the HOMO (π_A) of CO_2 (ψ_A^+ orbital in Figure 5). When the OCCO dihedral angle of the peroxide ring is twisted by about 90°, the unpaired electron finally occupies the π^* orbital of carbonyl fragment and the LUMO (π_S) of CO_2 (ψ_S^+ orbital). Note that the subscripts A and S denote the phase relations on the CO_2 molecule, which are antisymmetric and symmetric with respect to the mirror plane. Since such a conversion of the ET diradical configuration is formally correlated with the electronic motion from bonding (ψ_S^+) to antibonding (ψ_A^+) orbital, this conversion also invokes concomitant C−C bond breaking. The unpaired electron is gradually populated on the side of the carbonyl π^* orbital by favorable energetics; that is, the back transfer of negative charge from the CO_2 fragment begins at around $s = 4$ amu$^{1/2}$, as shown in Figure 2A (third). The MRMP calculations show that the S_0/S_1 energy gap along the IRC path is relatively small (about 15 kcal mol^{-1}) in region II because of a double excitation from the nonbonding orbital of the carbonyl group and the HOMO of the phenoxide group to the π^* orbital of the carbonyl group, as shown in Figure 2A; however, the electronic conversion is still adiabatic in view of the energy gap. The C−C breaking will occur smoothly without any electronic barrier.[43] The absence of an intermediary formation of the ET diradical is not trivial at all, because a long life intermediate is not only responsible for an intersystem crossing to generate the triplet state in region II, where the S_0 and T_1 states are near-degenerate, but also the source of hazardous radical reactions in biological systems.

(C) Region III: Back CT from the CO_2 Fragment. Let us extend the IRC analysis on the thermal CT reaction of *meta*-**1c** into region III (s > 5 amu$^{1/2}$ bohr). In this region, the C−C bond dissociation forms two fragments, i.e., *meta*-oxybenzaldehyde **5** and CO_2. As is observed in Figure 2A, region III is marked by spin annihilation ($y_{HOMO} \rightarrow 0\%$) and back CT from the CO_2 fragment ($\rho_{CO2} \rightarrow 0$). These events are already triggered by the orbital crossing between the HOMO (ϕ) and LUMO (ϕ^*) before the system enters region III, as shown in Figure 2B, because of the symmetry-forbidden [2 + 2] retrocyclic reaction. If the back CT occurs, the ET-diradical configuration (a singly excited configuration from the HOMO of the phenoxide group to the carbonyl π^* orbital) diabatically correlates with the excited configuration of products, while the closed-shell ground-state configuration of products correlates with the excited configuration of the ET diradical, as shown by the black dotted lines in Figure 2A. Due to the avoided crossing between these configurations, adiabatic surfaces are obtained, as shown by the black solid (S_0) and red dotted (S_1) lines. Mechanistically significant, the energy gap between the two surfaces is small, such that nonadiabatic transitions are possible. The Landau−Zener model[44] for this transition in the avoided crossing region has the form shown in eq 5, in which s is the slope of the unperturbed potential curves at the crossing point (r_0), v the velocity at r_0, and V_{01} one-half of the splitting between the actual potential curves at r_0.

$$p_{LZ} = \exp\left(-\frac{2\pi {V_{01}}^2}{\hbar v|s_0 - s_1|}\right) \qquad (5)$$

Therefore, the vast exothermicity for the initial O−O dissociation of *meta*-**1c** and the large difference between the S_0 and S_1 slopes at r_0 in Figure 2A are consistent with the high surface-hopping probability at the close proximity of the two states. Note that the rapid increase of the S_1 energy level after the avoided crossing (s > 6 amu$^{1/2}$ bohr) may be due to the use of the S_0 geometry in the MRMP calculations, since the S_0 geometry changes drastically at around the avoided crossing. This point will be mentioned again in the next section (see, for example, Figure 6).

In summary, the thermal CT reaction of *meta*-**1c** takes place by an asynchronous two-stage pathway without a well-defined diradical intermediate. The reaction is initiated by the irreversible O−O bond breaking, in which the electron-rich group operates by favoring the endothermic CT process (region I). Full one-electron transfer is achieved at the completely O−O cleaved geometry (region II). Then, the back CT process caused by the

(43) The difference in this point between the simple alkyl and phenoxide-anion-substituted dioxetanones is very striking. In the thermolysis of the parent and methyl-substituted dioxetanones **1a** and **1b**, the decomposition reactions are initiated by homolytic O−O breaking with activation energies of 16.0 and 16.3 kcal mol^{-1} after ZPC, as calculated at the B3LYP/6-311+G(d) level, and discrete singlet or triplet 1,4-diradical intermediates are formed on the reaction pathways, in which the oxygen lone pairs play crucial roles. The C−C bond breaking also demands an energy barrier of about 3−4 kcal mol^{-1}. In contrast, the addition of a phenoxide-anion group gives rise to the CT process, which corresponds to the nonstepwise mechanism; that is, no intermediate is formed.

(44) (a) Landau, L. D. *Phys. Zts. Sowiet.* **1932**, *2*, 46. (b) Zener, C. *Proc. R. Soc. London, Ser. A* **1933**, *137*, 696.

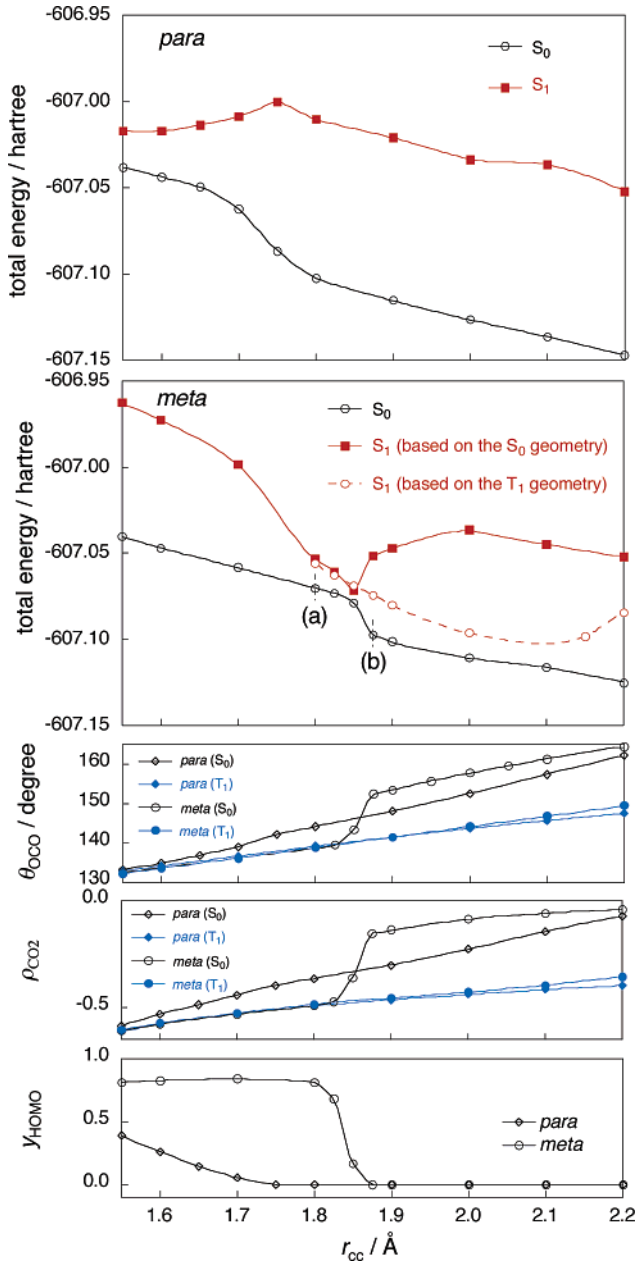

Figure 6. Energy profiles of the S_1 and S_2 states for the C−C bond-dissociation process of *para*-**1c** (top) and *meta*-**1c** (second), calculated by MRMP{12,11}$_{CC}$/6-31+G(d)//B3LYP/6-31+G(d); variations of the $O_4-C_2-O_5$ bending angle (θ_{OCO}) along the minimum-energy paths (third) optimized by B3LYP; variations of the total Mulliken charge densities of the CO_2 moiety (ρ_{CO2}) along the minimum-energy paths calculated by B3LYP (fourth); variations of the diradical character (y_{HOMO}) in the ground state along the minimum-energy paths calculated by B3LYP (bottom).

C−C bond breaking is responsible for the possibility of the nonadiabatic process for the direct generation of the excited state, that is, the concerted CTIL process is still possible (region III).

Origin of Odd/Even Selection Rule. The odd/even selection rule has been experimentally confirmed for the chemiluminescence properties of dioxetanes with regioisomeric aromatic fluorophores.[15,19−21] Half-lives for the decomposition of dioxetanes with an even-patterned aromatic fluorophore (*para* isomer) are usually shorter than those with an odd-patterned fluorophore (*meta* isomer), and the excitation yields for odd pattern are much higher than those for even pattern. We discuss the origin of this experimental observation in this section for *meta*-**1c** (odd) and *para*-**1c** (even); the IRC results of *para*-**1c** are more or less similar to those for *meta*-**1c**.[45]

Since the initial O−O bond dissociation is the rate-determining step for the thermal CT reaction of triggered dioxetanes and dioxetanones, the decomposition rates should have relevance to the primary CT process. Indeed, the observed dependency of the substitution pattern on the oxidation potential[11−14] is consistent with the reactant-like TS. The best account for the relationship between the substitution pattern and the half-life may be found in the interaction between the HOMO of the phenoxide anion and the σ^* orbital of the O−O bond, i.e., the magnitude of the MO coefficient at the C_6 of the aryl group attached to the dioxetane or dioxetanone ring.[21a] This orbital overlap is one of the controlling factors for the effective stabilization of the CT TS according to eqs S4 and S6. Our B3LYP calculations on the simple model system **1c** show the stronger CT interaction for *para*-**1c** than *meta*-**1c**, as observed in the ρ_{DON} values and the shapes of NOs at the CT TSs (see Figure S8 for *para*-**1c** and Figure 2 for *meta*-**1c**). The activation barriers for the CT reaction of *para*-**1c** are slightly lower than those of *meta*-**1c** by 1.6, 1.3, and 0.4 kcal mol^{-1} without ZPC, with ZPC, and with ZPC + approximate spin projection.

Frequently, the odd/even relationship for chemiluminescence efficiency has been explained in terms of the CIEEL stepwise mechanism,[15b,46] i.e., the relationship between the singlet quantum yield and the energy balance of the back ET between the solvent-caged neutral radical/radical ion pair. This is indeed a good account of the selection rule, but it does not go far enough in view of the dramatic difference ($>10^2$) in the excitation yield. Especially, the high quantum yields for the *meta* regioisomers are in conflict with the intermediary formation of solvent-caged species, since the diffusion from the cage[15] and the intersystem crossing in the radical pair[47] may effectively compete with the back ET process. This requires further explanations, i.e., in terms of the concerted CTIL process. McCapra[18b] provided a qualitative and pictorial description for the excitation channel, assuming a concerted mechanism; the $\pi\pi^*$ singlet excited state emerges more effectively in *meta*-directing systems immediately from a ground-state intramolecular CT species. Our ab initio calculations predict that the reaction proceeds in a two-stage pathway via the ET-diradical region. It follows that the back CT process in the C−C bond dissociation step for the generation of the ET diradical plays a crucial role in the local excitation of an electron donor. We previously presented a qualitative configuration interaction model for the direct generation of the electronically excited state in the back CT process.[9] The content of the model is briefly reviewed in the Supporting Information.

Potential-energy surfaces in the back CT region were explored by using the B3LYP and MRMP methods with the 6-31+G(d) basis set. We first computed the minimum-energy paths of the S_0 and T_1 states for the C−C bond dissociation process of the model dioxetanones *para*-**1c** and *meta*-**1c** by the partial optimization at the B3LYP level, in which only the C−C bond

(45) The results of the IRC analysis for *para*-**1c** are given in Figure S8 (Supporting Information).
(46) (a) Stevani, C. V.; Silva, S. M.; Baader, W. J. *Eur. J. Org. Chem.* **2000**, 4037. (b) Silva, S. M.; Wagner, K.; Weiss, D.; Beckert, R.; Stevani, C. V.; Baader, W. J. *Luminescence* **2002**, *17*, 362.
(47) Burshtein, A. I. *Chem. Phys.* **2003**, *289*, 251.

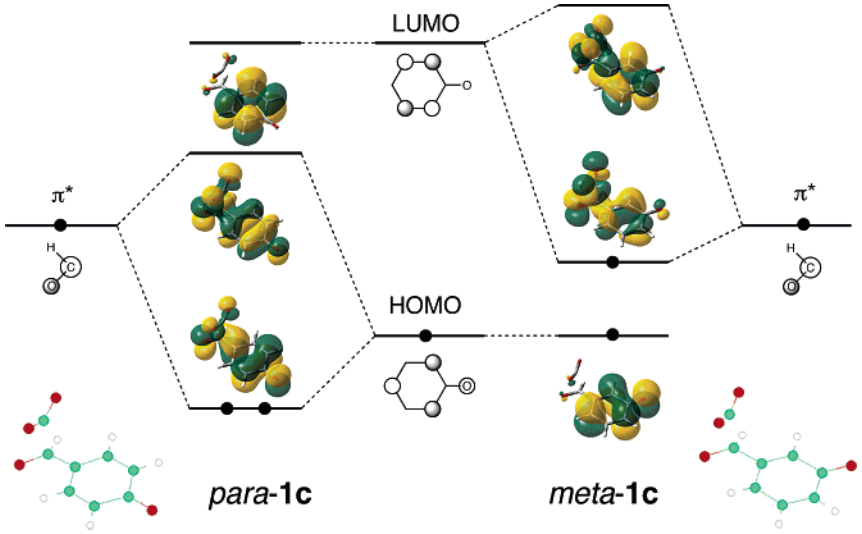

Figure 7. Schematic illustration of the MO correlation diagram of *para*-**1c** and *meta*-**1c** (r_{CC} = 1.9 Å); C, O, and H atoms are shown in green, red, and gray.

length was fixed at a given value.[48] Next, we carried out single-point energy calculations based on the S_0 and T_1 optimized geometries by the MRMP method to investigate the topographical features of the first excited state. The top and second panels in Figure 6 summarize the variations of the MRMP//B3LYP energies of the S_0 and S_1 states of *para*-**1c** and *meta*-**1c** against the C−C bond length (r_{CC}).[49] From third to bottom, the changes of the bending angle of $O_4-C_2-O_5$ (θ_{OCO}), net Mulliken charge density of the CO_2 moiety (ρ_{CO2}), and the diradical character (y_{HOMO}) in the ground-state calculated by B3LYP are shown as a function of r_{CC}. These results definitely indicate the difference between the *para* and *meta* regioisomers.

In *para*-**1c**, the various changes observed in the C−C bond dissociation is gradual. The S_0 energy monotonically decreases with increasing C−C bond length (top panel), and the accompanying geometrical change is also gradual, as representatively shown in the angle θ_{OCO} (third panel), which changes from bent ($\theta_{OCO} \cong 130°$) to linear ($\theta_{OCO} = 180°$) at the dissociation limit ($r_{CC} = \infty$). The negative charge developed on the CO_2 fragment is transferred to the *para*-oxybenzaldehyde and finally becomes zero (second from the bottom). The diradical character (y_{HOMO}) in the S_0 state is weak (<40%) in the short C−C bond-distance region (r_{CC} < 1.75 Å) and disappears at around r_{CC} = 1.75 Å (bottom panel). In this region, the S_1 state is well dominated by a double excitation from the nonbonding orbital of the carbonyl group and the HOMO of the phenoxide group to the π^* orbital of the carbonyl group, and the S_0/S_1 energy gap is relatively small (about 15 kcal mol^{-1}); however, the S_1 energy level markedly increases as the C−C bond cleaves (top panel), so that the nonadiabatic dissociation of *para*-**1c** should be rare. The reaction will proceed smoothly to the ground-state products.

In contrast, for the *meta*-**1c**, there is a weakly avoided crossing point between the S_0 and S_1 potential-energy curves at around r_{CC} = 1.85 Å (second panel). The S_0/S_1 energy gap at this point is only 4.6 kcal mol^{-1}, computed at the MRMP level. As a result, the sudden changes in both the S_0 and S_1 states are recognized in the very limited region of 1.8 < r_{CC} < 1.9 Å, although the change in the T_1 state is gradual; the large geometrical change (e.g., $\Delta\theta_{OCO} = 13.7°$) is followed by the drastic back CT ($\Delta\rho_{CO2} = 0.35$) and the spin annihilation ($\Delta y_{HOMO} = -81\%$) in the S_0 state, and the S_1 energy level rapidly falls and rises. To avoid the influence of the drastic S_0 geometrical change on the S_0/S_1 excitation energy, we also calculated the S_1 energy level along the T_1 minimum-energy path, as shown by the dashed line in the second panel. In this case, the S_1 energy level steadily decreases after the avoided crossing. This in turn implies that the drastic geometrical change in the S_1 state is not favorable. The interstate coupling will be large at the close proximity of the two states and will facilitate the nonadiabatic dissociation of *meta*-**1c** for producing the electronically excited fragment.

To clarify the origin of the difference between the *para* and *meta* regioisomers, we depict the HOMO, LUMO, and LUMO+1 of *para*-**1c** and *meta*-**1c** with the C−C bond distance of 1.9 Å, as shown in Figure 7. In *para*-**1c**, the π^* orbital of the carbonyl group interacts with the HOMO of the phenoxide group, while the overlap between the π^* orbital of the carbonyl group and the LUMO of the phenoxide group is negligible due to the orbital symmetries. This indicates that the *para*-**1c** easily collapses from the ET-diradical state to the ground state in the back CT region, in accordance with the large S_0/S_1 gap in Figure 6 (top). On the contrary, the behavior of the *meta*-**1c** is reversed: the π^* orbital of the carbonyl group predominantly interacts with the LUMO of the *meta*-substituted phenoxide group, which increases the mixing between the ET and locally excited configurations in eq S8 (see Supporting Information). This process in the back CT region results in the nonadiabatic back CT process for the local excitation of the phenoxide group and will enhance the chemiluminescence efficiency. The odd/even selection rule for the excitation yield is well substantiated by both the orbital symmetry rule and ab initio calculations, in terms of the concerted CTIL mechanism.

Possibility of the CIEEL versus the Concerted CTIL Mechanism. Up to this point, we have been concerned with

(48) The obtained minimum-energy paths are considerably different from the IRC paths; for example, the OCCO ring for the minimum-energy paths is twisted by 50−55° for *para*-**1c** and 80−90° for *meta*-**1c**, while the IRC paths retain approximately planar structures. We believe that most of the finite temperature pathways will lead to the twisted structure valley, since the potential-energy surface along the IRC path is downhill toward the motion corresponding to the rotation of the CO_2 moiety.

(49) Energy profiles of the S_0 and T_1 states of *para*-**1c** and *meta*-**1c** calculated by the B3LYP method are shown in Figure S9 (Supporting Information).

the stationary-state quantum mechanics of isolated molecules. Such a treatment invariably involves the LUMO−LUMO or LUMO−HOMO interaction for the back CT. We must notice, however, that (i) conformational changes and molecular deformations other than the IRC path play crucial roles and (ii) most of chemiluminescence reactions occur in solutions. Solvents may have an effect on the decomposition rates and the course of the reactions. In this section, we discuss the possibility of the CIEEL mechanism more closely in connection with the effects of the CO_2 bending vibration mode and the solvent polarity.

(A) Importance of the CO_2 Bending Vibration. According to the simple MO picture, the excitation mechanism of *meta*-**1c** is formally described in terms of the movement of one unpaired electron to the dioxetanone functionality. At the 90° twisted structure with a short C−C distance, the unpaired electron enters the π^* orbital of carbonyl group and the LUMO (π_S) of the CO_2 fragment, as shown in Figure 5. If the unpaired electron is accidentally localized on CO_2 in the C−C bond dissociation step, the neutral radical of *meta*-oxybenzaldehyde **5** and anion radical of CO_2 are produced. In this case, the CIEEL process is completed by the subsequent intermolecular ET to give excited-state *meta*-**5** and ground-state CO_2 (see Scheme 1). On the other hand, if the unpaired electron is delocalized into the LUMO of the phenoxide group due to the strong π^*−LUMO interaction, excited *meta*-**5** is directly formed on the decomposition pathway of *meta*-**1c** (concerted CTIL process). After all, the bifurcation of the excitation route rests on the balance between the electron-accepting ability of *meta*-**5** and CO_2.

In this context, we have computed the electron affinity of CO_2. The optimized geometries of ground-state CO_2 and the CO_2 anion in the gas phase were determined by B3LYP/6-311+G(d). Charged CO_2^- has a bent structure in the ground state with the CO distance of 1.231 Å and O−C−O angle of 137.8°, while a linear structure with the CO distance of 1.161 Å is given for neutral CO_2. The potential-energy curves of CO_2 and CO_2^- as a function of O−C−O deformation angle (θ_{OCO}) indicate that the one-electron capture process is endothermic at the linear-like geometry ($\theta_{OCO} > 153°$), while the bent structure ($\theta_{OCO} < 153°$) gives a large positive vertical electron affinity (Figure S10). This is caused by the sensitivity of the energy levels of the asymmetric HOMO (π_A) and symmetric LUMO (π_S) to the symmetric bending vibration of CO_2. The O−C−O bending vibration has a strong influence on the electron capture ability of CO_2. In fact, the third and fourth panels in Figure 6 show the close correlation between θ_{OCO} and ρ_{CO2}. Although the gas-phase calculations provide a negative adiabatic electron affinity of CO_2, it turns positive in the solution phase because of the much larger solvation energy of the charged CO_2^- species. For example, the solvation free energies (ΔG_{solv}) of CO_2 and CO_2^- in benzene (DMSO) at 298.15 K are 0.64 (0.065) and −33.3 (−59.9) kcal mol^{-1}, as determined by the PCM HF/6-31+G(d) method. For comparison, ΔG_{solv} is −1.1 (−3.6) and −29.3 (−56.5) kcal mol^{-1} for the neutral radical and anion states of *meta*-**5** in benzene (DMSO).

To examine the accessibility of the CIEEL route, we considered the $O_4-C_2-O_5$ bending vibration mode of *meta*-**1c**, which is orthogonal to the C−C dissociation minimum-energy path. Partial geometry optimization was performed by fixing the two parameters r_{CC} and θ_{OCO}; r_{CC} was fixed at 1.8 or 1.875 Å before or after the avoided crossing point [(a) or (b) in Figures 6 and S9], and θ_{OCO} was varied from 130° to 155°. Single-point calculations were carried out by PCM B3LYP/6-31+G(d),[50] in which the thermal contribution was omitted, to evaluate the free-energy change in the benzene ($\epsilon = 2.25$) and DMSO ($\epsilon = 46.70$) media. As shown in Figure 8, the results demonstrate that the behavior of the potential-energy surface is largely dependent on the r_{CC} and θ_{OCO} parameters of the substrate and dielectric property of a solvent.

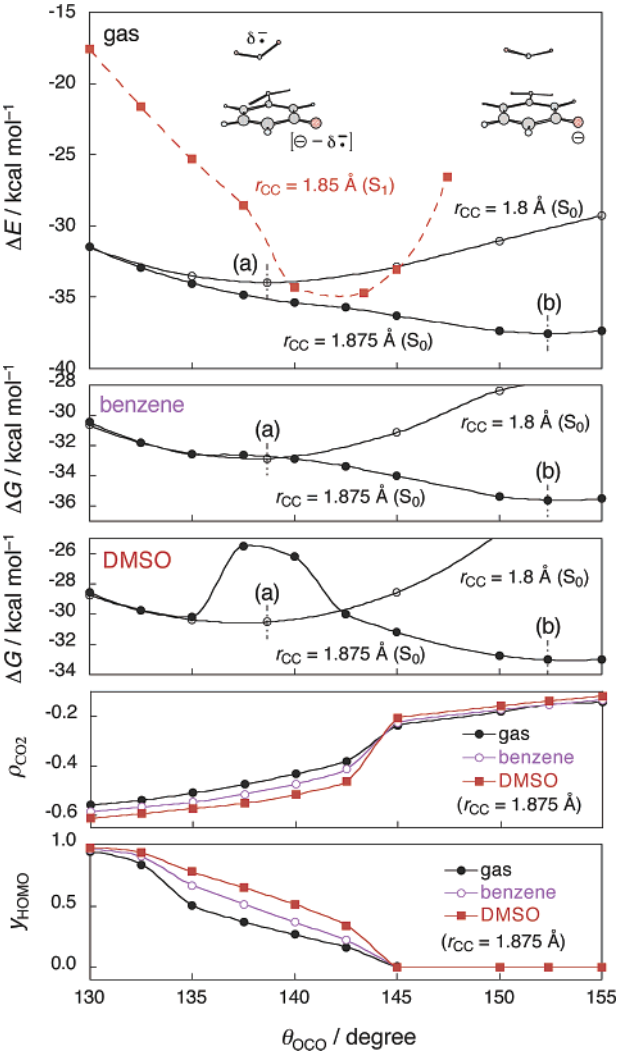

Figure 8. Energy profiles of the S_0 minimum-energy paths ($r_{CC} = 1.8$ and 1.875 Å) and the S_1 energy changes along the S_0 minimum-energy path ($r_{CC} = 1.85$ Å) for the $O_4-C_2-O_5$ bending vibration mode of *meta*-**1c** in the gas phase (top), benzene (second), and DMSO (third) media, as calculated by PCM B3LYP/6-31+G(d); the adiabatic excitation energies between the structure at point (a) and the structures for $r_{CC} = 1.85$ Å were calculated by the MRMP{12,11}$_{CC}$/6-31+G(d) method; variations of the total Mulliken charge densities of the CO_2 group (ρ_{CO2}) along the minimum-energy path ($r_{CC} = 1.875$ Å) (fourth); variations of the diradical character (y_{HOMO}) along the minimum-energy path ($r_{CC} = 1.875$ Å) (bottom).

In the gas phase (top panel in Figure 8), for the most stable conformation, the O−C−O angle shifts from 138.7° (a) to

(50) The HF method should be chosen for the reliable calculations of solvation free energies, since the parameters of the PCM (or more specifically, UAHF PCM) model were optimized for the HF/6-31+G(d) level of theory;[33d] however, the HF method tends to overestimate the diradical character ($y_{HOMO} > 90\%$) for the back CT region, characterized by the B3LYP method, and provides biased results in favor of diradical pathway (see Figure S2). Therefore, the calculations for the back CT region as well as the CT TSs were conducted using the B3LYP method.

152.4° (b), as the C−C bond is elongated from 1.8 to 1.875 Å. The system undergoes barrierless motion from the ET diradical ($y_{HOMO} \cong 80\%$) to the nonradical species ($y_{HOMO} = 0\%$) in the S_0 state. The accompanying back CT is responsible for the generation of ground-state or locally exited-state configuration, according to eq S8. Judging from the shape of the potential surface, the radical dissociation for producing the CO_2 anion radical with bent structure and neutral radical of *meta*-**5** may scarcely occur in the gas phase.

PCM calculations predict that the solvent polarity provokes a significant change in the curvature near the back CT region. As shown in the second and third panels in Figure 8, a shoulder zone with a nearly float slope or a small energy barrier appears on the S_0 potential curve ($r_{CC} = 1.875$ Å) in nonpolar (benzene) and polar (DMSO) media. This is attributable to the difference in the solvent stabilization between the ET diradical and nonradical species;[51] that is, the solvent polarity tends to accumulate the negative charge on the CO_2 fragment and promote the radical dissociation. The ρ_{CO2} and y_{HOMO} values, which provide a chemical criterion for the formation of a diradical by one-electron transfer, support this tendency, as shown in the fourth and bottom panels of Figure 8; for example, the ρ_{CO2} values for $\theta_{OCO} = 135°$ ($r_{CC} = 1.875$ Å) in the gas, benzene, and DMSO media are −0.51, −0.54, and −0.57, and the corresponding y_{HOMO} values are 50.7, 66.8, and 77.5%. These results imply some possibility of skipping over the back CT region to form a solvent-caged radical pair or free radicals in the solution-phase decomposition, which increase with increasing solvent polarity. That is, the CIEEL mechanism may become effective in solutions. The vicinity of the weakly avoided crossing region provides a branching point for the CIEEL or concerted CTIL excitation route, which is largely characterized by the timing of the CO_2 bending vibration. Such a mechanistically borderline feature is manifested in the shape of the potential-energy curves in the second and third panels of Figure 8. In the benzene medium, some trajectory may run on to the shoulder zone at around $\theta_{OCO} = 135°$ and narrowly trace a radical dissociation pathway to generate radical species. Most trajectories, however, will follow a downhill pathway that leads to a weakly avoided crossing region, in which nonadiabatic back CT may occur due to the strong LUMO−LUMO interaction as shown in Figure 7. In the DMSO medium, nevertheless, the dissociation valley to form radicals definitely appears at the CO_2 bent structure ($\theta_{OCO} \cong 135°$). This implies that the formation of solvent-caged radicals or even free radicals may be promoted by solvent polarity. The polarization-induced branching excitation mechanism is applicable to the solution-phase CT reaction of the dioxetanone model system *meta*-**1c**.

(B) Solvent Effects on Energetics. The final decomposition products were also optimized in benzene and DMSO by PCM with B3LYP/6-31+G(d), except for the CO_2 anion, which was optimized by the Onsager model with B3LYP/6-31+G(d). All products were treated as separate molecules surrounded by a medium of continuous dielectric. The optimized geometries in solutions do not differ much from the gas-phase geometries.[52] Although we could not obtain detailed information on the intermediary stages,[53] the energetics of the final products provides some insights into the back ET process. Figure 4B summarizes the free energies (ΔG) of the CT TS and products relative to the equilibrium structure of *meta*-**1c** in the gas and solution phases, according to eq 4. Evidently, the neutral−ionic radical pair, i.e., neutral radical of *meta*-**5** and anion radical of CO_2 (S_0' state), is much more strongly stabilized than other combinations of products on going from the gas to solution phase.[55] This implies that polar solvent molecules may effectively rearrange in response to the charge distribution in the neutral−ionic radical pair and reduce the free energy of activation for the radical dissociation in the bulk medium. In this case, the released two doublet molecules will randomly diffuse and eventually react with solvent or collide to generate a triplet radical pair about three times more effectively than singlet radical pair; therefore, the chemiluminescence efficiency will be reduced. In contrast, the ET rate for the formation of the triplet or singlet excited state from the solvent-caged radicals may be relatively slow in the polar medium, because the solvation free energy of T_1 products, which presumably have a similar charge distribution to that of S_1 products, is less negative than those of the other states.

In summary, the CIEEL mechanism may be realized in the solution-phase decomposition because of the surface bifurcation near the back CT region; however, the solvent polarity is predicted to be disadvantageous for the efficiency of the back ET process.[55] There are other modes that may render the CIEEL process more efficient. The cage escape is sensitive to the viscosity of the reaction medium,[15] and the intersystem crossing may occur in the solvent-caged radical pair before the final spin annihilation.[47] Actually, the CIEEL efficiency will be largely affected by the kinetic factors for the competitive pathways, which are highly dependent on the employed conditions. A molecular dynamic simulation would be desirable in the further discussion of the branching ratio for the various reaction pathways and the estimation of quantum yields.

Conclusions

The mechanisms of the thermal CT decomposition of phenoxide-anion-substituted dioxetanones **1c** as model molecules of the highly efficient chemi- and bioluminescence systems such as AMPPD **4** and the dioxetanone intermediate **3** of firefly luciferin, as shown in Figure 1, have been investigated by the hybrid DFT and MRMP methods. The electron-donating functionality (trigger in Figure 1) drastically determines the

(51) For reference, the solvation free energies of (a) the strong ET diradical and (b) the nonradical points in benzene (DMSO) were calculated to be −24.1 (−46.7) and −23.2 (−45.7) kcal mol^{-1}.

(52) We also tried to locate the equilibrium structures (min.) and the CT TSs of *para*- and *meta*-**1c** in benzene and DMSO at the PCM (for min.) or Onsager model (for CT TSs) B3LYP/6-31+G(d) levels. It was found that, despite the presence of the solvent reaction field, there are insignificant changes in the equilibrium geometries; however, the relatively large structural change of the CT TS on going from the gas phase to a solution is made explicit in the O−O distance and is largely dependent on the degree of solvent polarity. The detailed results are summarized in Table S3 (Supporting Information).

(53) In the CIEEL mechanism, it is assumed that the excitation process takes place within the encounter complex, which may be described as an intermolecular ensemble of the solvent-caged radical pair, usually separated by a small distance (~7 Å).[54] Then, the collisional contact between the partners is assumed to form a collision complex, in which the ground, singlet excited, or triplet states of an emitter may be produced, if the ET occurs immediately during the lifetime of the collision complex.[15a]

(54) Kavarnos, G. J.; Turro, N. J. *Chem. Rev.* **1986**, *86*, 401.

(55) The main reason for this can be attributed to the small size of the CO_2 molecule, since the Born equation predicts that the solvation free energy is strongly negative for small, highly charged ions in media of large dielectric constants. Thus, the trend of *meta*-**1c** reported in this article does not always apply to other intramolecular CIEEL systems. In the case of AMPPD **4**, for example, ΔG_{solv} [−30.5 (−57.2) kcal mol^{-1} in benzene (DMSO)] of the adamantanone anion is less negative than that [−30.9 (−60.5) kcal mol^{-1}] of the methyl *meta*-oxybenzoate anion at the PCM HF/6-31+G(d)//B3LYP/6-31+G(d) level.

chemiluminescence activity. The deprotonation of the phenolic OH group of the neutral form **1d** causes a change in the nature of the TS from homopolar 1,4-diradical to intramolecular CT diradical, thereby lowering the activation energy substantially; however, the CT TS is still endothermic. The triggering changes the reaction mechanism from stepwise to one without a discrete intermediate. The nonstepwise mechanism prevents some side reactions, e.g., the intersystem crossing to triplet state, which is responsible for lowering the efficiency and radical reactions with the environment. The electron-acceptor functionality (energy source in Figure 1) is relevant for optimizing the chemiluminescence activity. Much larger energy released by the dioxetanones than the dioxetanes may be utilized not only for the efficient formation of excited products but also to accelerate the rate of the chemiluminescence process. The structure of the aromatic fluorophore, i.e., the *para*- and *meta*-orientation between the donor (oxyanion) and acceptor (peroxide) functionalities, strongly influences the excitation yield; thus, the *meta* regioisomer is much very effective. Qualitative consideration and ab initio calculations both support that the much higher excitation yield of the *meta*-isomer stems from the orbital interaction for the nonadiabatic back CT.

Compared to the concerted CTIL process, the CIEEL stepwise mode is subject to reduction of the excitation yield due to inherent side reactions, such as intersystem crossing to nonluminescent triplet states and escape from solvent cage. Our calculations provide a borderline mechanistic dichotomy for the thermal CT of *meta*-**1c**: in addition to the concerted CTIL process (favored in the gas phase), the CIEEL process competes in the solution phase, so that for the reaction of *meta*-**1c** two competitive excitation routes apply, once the CT TS has been surpassed. The branching in these routes is characterized by the CO_2 bending vibration as the C−C bond begins to cleave; its surface bifurcation depends largely on the solvent polarity. The linear CO_2 structure leads to the nonadiabatic or adiabatic back CT, while the charge development on the CO_2 fragment for radical dissociation must accompany CO_2 bending, which is promoted by polar medium. Dynamic treatment, which includes the nonadiabatic electronic coupling and the medium effect, is required for understanding better the complex mechanism of such a borderline reaction.

Acknowledgment. We gratefully acknowledge the efforts of one of referees for clarifying key concepts of CIEEL and related electron-transfer reactions. His careful reading of the original manuscript led to many valuable comments, criticisms, and improvement for this paper. H.I. is indebted to the National Project on Protein Structural and Functional Analyses from the Ministry of Education, Culture, Sports, Science and Technology for their financial assistance. Y.T. is grateful to the Japan Society for the Promotion of Science (Research Fellowships of Japan Society for the Promotion of Science for Young Scientists) for financial support of this research.

Supporting Information Available: Theoretical details and confirmation of the methods used in this study are presented. The other data are as follows: solvent effects on the equilibrium state and CT TSs of **1c** (Table S3); total electronic energies and zero-point and thermal corrections for all structures reported (Tables S4); Cartesian coordinates of all structures reported (Tables S5); variations in the vertical electron affinity of dioxetanone and dioxetane skeletons (Figure S6); energy diagrams for the thermal CT decomposition of *para*-**1c** (Figures S7); IRC results of *para*-**1c** (Figure S8); potential-energy curves of *para*-**1c** and *meta*-**1c** by B3LYP (Figure S9); potential-energy curves of CO_2 species (Figure S10). This material is available free of charge via the Internet at http://pubs.acs.org.

JA043295F